# Synthesis, Structure, and Magnetic Properties of Three New One-Dimensional Nickel(II) Complexes: New Magnetic Model for the First One-Dimensional $S = 1$ Complex with Alternating Ferro-Ferromagnetic Coupling

**Montserrat Monfort,*[a] Immaculada Resino,[a] M. Salah El Fallah,[a] Joan Ribas,[a] Xavier Solans,[b] Mercé Font-Bardia,[b] and Helen Stoeckli-Evans[c]**

**Abstract:** Three new one-dimensional nickel(II) complexes with the formulas *trans*-$[Ni(N\text{-Eten})_2(\mu_{1,3}\text{-}N_3)]_n(ClO_4)_n$ (**1**), *trans*-$[Ni(N\text{-Eten})_2(\mu_{1,3}\text{-}N_3)]_n(PF_6)_n$ (**2**), and *cis*-$[Ni(N\text{-Eten})(\mu_{1,1}\text{-}N_3)_2]_n$ (**3**) (*N*-Eten = *N*-Ethylethylenediamine) were synthesized and characterized. Complex **1** has the $P2_1/c$ space group and consists of a structurally and magnetically alternating one-dimensional antiferromagnetic system with end-to-end azido bridges. Compound **2** has the $P\bar{1}$ space group and has alternate units in its structure but consists of a magnetically uniform one-dimensional antiferromagnetic system with end-to-end azido bridges. Complex **3** has the $I2/a$ space group and may be described as a structurally and magnetically alternating one-dimensional ferromagnetic system with double azido bridged ligands in an end-on coordination mode. The $\chi_M T$ versus $T$ plots for compound **3** suggest an intramolecular ferromagnetic interaction between adjacent $Ni^{II}$ ions and metamagnetism at low temperature (below 10 K). The magnetization measurements versus applied field confirm this metamagnetic ordering. In order to describe the magnetic data of this compound we developed a general formula for the magnetic susceptibility of the isotropic ferro-ferromagnetic $S = 1$ Heisenberg chain in terms of the alternation parameter $\alpha$ $(=J_2/J_1)$; this assumed a variation of $\chi_M T$ versus the length $N$.

**Keywords:** azides · magnetic properties · N ligands · nickel

## Introduction

Over the last few years, the design of one-dimensional magnetic materials has been an active area of research in coordination chemistry. There are several good reasons for this. The most important of these is that the position they occupy between high-nuclearity clusters and 3-D extended lattices provides new possibilities for understanding more phenomena that cannot be explained at a higher dimension. In fact, extended systems of a variety of metals and ligands have been characterized, and these provide very interesting information about magnetostructural correlations in these compounds.[1–4]

When we focus our attention on one-dimensional compounds with azido bridges, the large number of uniform or alternate antiferromagnetic systems and the number of alternate ferro-antiferromagnetic systems contrast with the paucity of ferromagnetic chains.[5] It is well-known that usually the end-to-end (EE) coordination mode of the azido bridge couple spins antiferromagnetically, while the end-on (EO) coordination mode couple spins ferromagnetically, but for very large M-$\mu_{1,3}$-$N_3$–M bond and torsion angles the magnetic coupling may be reversed.[6]

To our knowledge, all one-dimensional compounds with EE azido bridges or those containing simultaneously both kinds of coordination mode (EE and EO) show a global antiferromagnetic behavior.[5a] The only exception to this is $[\{Ni(5\text{-methylpyrazole})_4(\mu_{1,3}\text{-}N_3)\}_n](ClO_4)_n \cdot n H_2O$,[7] in which the torsion angle for the EE azido bridge is 75.7°; this is in the range where the antiferromagnetic contribution is minimized to favor the ferromagnetic contribution.[6] Only one 1-D compound with a double EO azido bridge and ferromagnetic coupling with $Mn^{II}$ ions has been studied in depth and characterized.[8] In this compound, three different manganese atoms are present along the chain. The sequence of these

[a] Prof. M. Monfort, Dra. I. Resino, Dr. M. S. El Fallah, Prof. J. Ribas
Departament de Química Inorgànica
Universitat de Barcelona
Martí i Franqués 1-11, 08028-Barcelona (Spain)
Fax: (+34) 93-4907725
E-mail: mmonfort@kripto.qui.ub.es

[b] Prof. X. Solans, Dra. M. Font-Bardia
Departament de Cristallografia i Mineralogia
Universitat de Barcelona
Martí i Franqués, s/n, 08028-Barcelona (Spain)

[c] Prof. H. Stoeckli-Evans
Institut de Chimie
Université de Neuchâtel
Av. de Bellevaux 51, 2000 Neuchâtel (Switzerland)



0947-6539/01/0701-0280 $ 17.50+.50/0

manganese ions forces four different bridges in the chain, and this results in alternating coupling constants. The similar bond parameters in the different bridges allow the magnetic results to be fitted to the conventional equations[9] due to the absence of a model for this complicated system. Miller et al.[10] recently published work concerning a layer of ferromagnetic 1-D coupled $[Mn(\mu_{1,1}N_3)_2]$ chains bridged together with $\mu$-pyrazine. In this case, the $\chi_M T$ was fitted to the same conventional equation[9] for the evaluation of the ferromagnetic interaction through the azide ligands. This was done with one additional mean-field correction in order to assess the interchain antiferromagnetic interactions through the bridging pyrazine ligands. Previously, some of the authors reported two complexes of general formula $[Ni(L)(\mu_{1,1}\text{-}N_3)_2]$, (L = diamine).[11] In this case, the magnetic coupling was evaluated as an average value using the expression developed by T. de Neef for the uniform $S = 1$ ferromagnetic chain.[12]

Here, we report the synthesis, structure, and magnetic properties of three new one-dimensional compounds. Reacting the *N*-Eten (*N*-Eten = *N*-Ethylethylenediamine) with $Ni^{II}$ in the ratio 2:1, we obtain two free positions in the $Ni^{II}$ environment that can be occupied by the $N_3^-$ bridging ligand in the *cis* or *trans* position; this gives a cationic dinuclear compound or a 1-D cationic compound. Sometimes a mononuclear complex can appear.[7] Here, if this ratio has been applied, we have been able to separate two one-dimensional compounds, *trans*-$[Ni(N\text{-Eten})_2(\mu_{1,3}\text{-}N_3)]_n(ClO_4)_n$ (**1**) and *trans*-$[Ni(N\text{-Eten})_2(\mu_{1,3}\text{-}N_3)]_n(PF_6)_n$ (**2**), in which the $Ni^{II}$ ions are bridged by one azido ligand in the EE mode. In compound **1**, two different azido bridges are present in the chain. The $Ni^{II}$ ions are related by an inversion center located in the central nitrogen of each azido bridge; this means that the compound has a structurally and magnetic alternating antiferromagnetic chain. Compound **2** shows the same distribution around the $Ni^{II}$, but in this case two different $Ni^{II}$ ions are present, located in an inversion center; all the azido bridges are equivalent, and this gives a structural antiferromagnetic uniform chain.

Otherwise, if the ratio is changed to 1:1 for amine:$Ni^{II}$, four positions around the $Ni^{II}$ are free and can be occupied by the $N_3^-$ ligand, and this gives a neutral $[Ni(N\text{-Eten})(\mu_{1,1}\text{-}N_3)_2]_n$ (**3**) compound, in which the $Ni^{II}$ ions are bridged by two azido ligands, in the EO mode. All the $NiN_6$ octahedra are equivalent, but alternatively the $Ni^{II}$ ions are related by an inversion center or by a binary axis; this sequence leads to a structural and ferromagnetic alternating chain.

A large number of suitable models have been developed to explain and quantify the magnetic alternation in the linear 1-D compounds. Hatfield et al.[13] have solved numerically the magnetic exchange for alternating antiferromagnetic chains of spin $S = 1/2$. In the same way, other new expressions have been developed to evaluate the magnetic susceptibility for $S = 1/2$ chains with alternating ferro- and antiferromagnetic exchange couplings, and $S = 1$ alternating antiferromagnetic or alternating ferro-antiferromagnetic chains.[14, 15] In contrast, no analytical expression has yet been proposed for the magnetic susceptibility of $S = 1$ chains, which are characterized by simultaneously different ferro and ferromagnetic couplings. Therefore, we felt it appropriate to extend those calculations and attempt to develop such an expression.

**Abstract in Catalan:** *S'han sintetitzat i caracteritzat tres nous compostos monodimensionals de níquel(II) de fórmula trans-[Ni(N-Eten)$_2$($\mu_{1,3}$-N$_3$)]$_n$(ClO$_4$)$_n$ (**1**), trans-[Ni(N-Eten)$_2$($\mu_{1,3}$-N$_3$)]$_n$(PF$_6$)$_n$ (**2**) i cis-[Ni(N-Eten)($\mu_{1,1}$-N$_3$)$_2$]$_n$ (**3**), (N-Eten = N-Ethylethylenediamine). El compost **1** cristal·litza en el grup P2$_1$/c i consisteix en un sistema monodimensional antiferromagnètic amb ponts azidur "end-to-end" alternat tant estructural com magnèticament. El compost **2** cristal·litza en el grup P$\bar{1}$ i consisteix també en un compost monodimensional antiferromagnètic amb ponts azidur "end-to-end" alternat estructuralment, però uniforme des del punt de vista magnètic. El complex **3** cristal·litza en el grup I2/a i es pot descriure com un sistema monodimensional ferromagnètic, alternat tant estructural com magnèticament amb dobles ponts azidur amb el mode de coordinació "end-on". Les gràfiques de $\chi_M T$ respecte a T per aquest últim compost suggereixen una interacció intramolecular ferromagnètica entre ions Ni$^{II}$ veïns i metamagnetisme a baixes temperatures (per sota 10 K). Les mesures de magnetització respecte el camp, confirmen aquest metamagnetisme. Per tal de descriure i interpretar els valors magnètics obtinguts, hem desenvolupat una fórmula general per la susceptibilitat magnètica per a cadenes isotropiques S = 1 tipus Heisenberg alternades ferro-ferromagnèticament en funció del paràmetre d'alternança $\alpha$ ($=J_2/J_1$), assumint la variació de $\chi_M T$ en funció de la longitud N.*

## Results and Discussion

### Description of the structures

*trans*-$[Ni(N\text{-Eten})_2(\mu_{1,3}\text{-}N_3)]_n(ClO_4)_n$ (**1**): The structure consists of cationic chains of nickel atoms linked by EE azido bridges, isolated by $ClO_4^-$ anions found in the interchain space. The chain runs along the diagonal of the (0 1 0) plane (Figure 1). In the chain structure, each $Ni^{II}$ atom is coordinated by two bidentate *N*-Eten ligands and two azido ligands in a distorted octahedral *trans* arrangement. A labeled scheme of the cationic part is shown in Figure 2. The four N atoms of the diamine ligands and the $Ni^{II}$ atom are in the same plane. All the $Ni^{II}$ atoms are equivalent but they are linked by two different azido bridges and related by the inversion center located at the central nitrogen of the azido groups. This produces a structurally alternating chain. The two $Ni\text{–}N_{azido}$ distances are the shortest (1.863(4) and 1.884(3) Å), and the two longest distances are for two $Ni\text{–}N_{amine}$ coordinated to *Ethyl* ligands (2.0894(4) and 2.103(3) Å). The two bond angles related to the azido ligands are Ni–N1–N2 134.8(3) and Ni–N3–N4 143.7(4)°. Each fragment of five $Ni\text{–}N_3\text{–}Ni$ atoms is coplanar, and consequently the torsion angle is 180°. The main bond lengths and angles are listed in Table 1.

*trans*-$[Ni(N\text{-Eten})_2(\mu_{1,3}\text{-}N_3)]_n(PF_6)_n$ (**2**): This structure also consists of cationic chains of nickel atoms linked by EE azido bridges, isolated by $PF_6^-$ anions found in the interchain space.

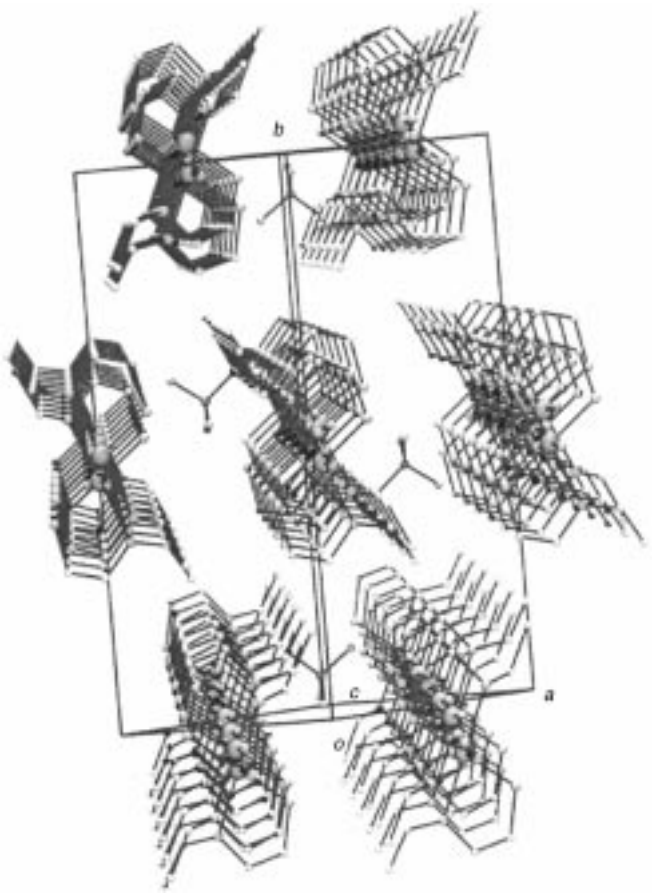


Figure 1. View of the unit cell of *trans*-$[Ni(N\text{-Eten})_2(\mu_{1,3}\text{-}N_3)]_n(ClO_4)_n$ (**1**). The hydrogen atoms are omitted for clarity.

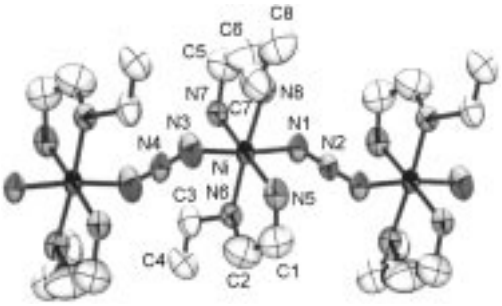


Figure 2. ORTEP drawing of the cationic part of *trans*-$[Ni(N\text{-Eten})_2(\mu_{1,3}\text{-}N_3)]_n(ClO_4)_n$ (**1**) that shows atom labeling scheme. Ellipsoids at the 50% probability level.

Table 1. Selected bond lengths [Å] and angles [°] for $[Ni(N\text{-Eten})_2(\mu_{1,3}\text{-}N_3)]_n(ClO_4)_n$ (**1**).

| | | | |
|---|---|---|---|
| Ni–N1 | 1.884(3) | Ni–N3 | 1.863(4) |
| Ni–N5 | 1.989(4) | Ni–N6 | 2.103(3) |
| Ni–N7 | 1.971(4) | Ni–N8 | 2.089(4) |
| N3–Ni–N1 | 173.2(2) | N3–Ni–N7 | 78.7(19) |
| N1–Ni–N7 | 95.9(15) | N3–Ni–N5 | 103.6(2) |
| N1–Ni–N5 | 82.0(15) | N7–Ni–N5 | 177.6(11) |
| N3–Ni–N8 | 95.2(16) | N1–Ni–N8 | 80.0(14) |
| N7–Ni–N8 | 80.45(14) | N5–Ni–N8 | 99.6(15) |
| N3–Ni–N6 | 89.4(16) | N1–Ni–N6 | 95.4(14) |
| N7–Ni–N6 | 100.5(13) | N5–Ni–N6 | 79.2(15) |
| N8–Ni–N6 | 175.4(10) | N2–N1–Ni | 134.8(3) |
| N4–N3–Ni | 143.7(4) | N3–N4–N3#2 | 180.0(1) |
| N1–N2–N1# | 180.0 | | |

The chain runs along the [0 0 1] direction (Figure 3). An ORTEP plot of the cationic part is shown in Figure 4. The main bond lengths and angles are gathered in Table 2. There

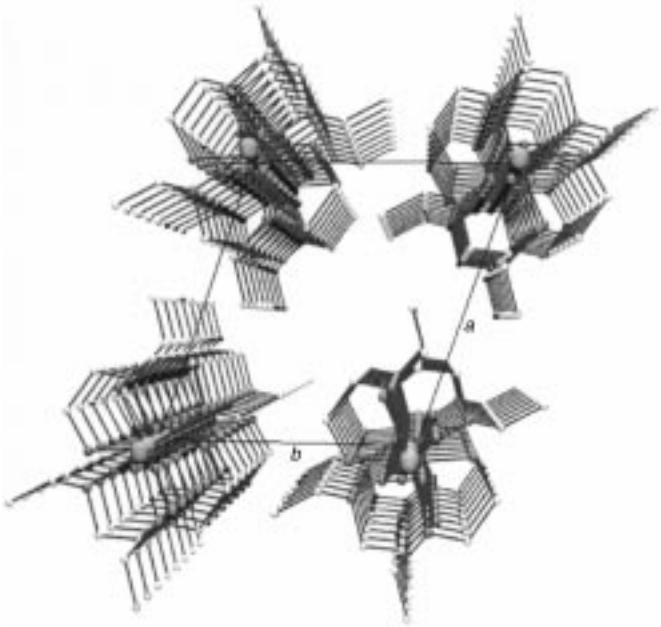


Figure 3. View of the unit cell of *trans*-$[Ni(N\text{-Eten})_2(\mu_{1,3}\text{-}N_3)]_n(PF_6)_n$ (**2**). The hydrogen atoms and $PF_6^-$ units are omitted for clarity.

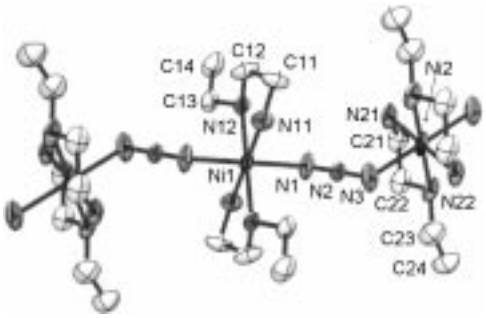


Figure 4. ORTEP drawing and labeling scheme of the cationic part of *trans*-$[Ni(N\text{-Eten})_2(\mu_{1,3}\text{-}N_3)]_n(PF_6)_n$ (**2**). Ellipsoids at the 50% probability level.

are two different $Ni^{II}$ in the chain located at the inversion center; this produces an alternating structural chain with only one kind of azido bridge. Each $Ni^{II}$ is surrounded by six nitrogen atoms; four of them belong to two diamines in *trans*

Table 2. Selected bond lengths [Å] and angles for $[Ni(N\text{-Eten})_2(\mu_{1,3}\text{-}N_3)]_n(PF_6)_n$ (**2**).

| | | | |
|---|---|---|---|
| Ni1–N1 | 2.152(3) | Ni2–N21 | 2.111(4) |
| Ni1–N11 | 2.073(4) | Ni2–N22 | 2.129(4) |
| Ni1–N12 | 2.148(4) | N1–N2 | 1.161(4) |
| Ni2–N3 | 2.153(3) | N2–N3 | 1.154(5) |
| N1–Ni1–N1#1 | 180.0 | N3–Ni2–N3#2 | 180.0 |
| N11–Ni1–N11#1 | 180.0 | N21–Ni2–N21#2 | 180.0 |
| N12–Ni1–N12#1 | 180.0 | N22–Ni2–N22#2 | 180.0 |
| N11–Ni1–N12#1 | 97.3(15) | N21–Ni2–N22 | 97.29(17) |
| N11–Ni1–N12 | 82.5(2) | N21–Ni2–N22 | 82.71(17) |
| N11–Ni1–N1 | 92.47(15) | N21–Ni2–N3 | 92.76(16) |
| N11–Ni1–N1#1 | 92.70(18) | N21–Ni2–N3#2 | 87.2(2) |
| N3–N2–N1 | 178.3(4) | N2–N1–Ni1 | 134.8(3) |
| N2–N3–Ni2 | 123.4(3) | | |



0947-6539/01/0701-0282 $ 17.50+.50/0 *Chem. Eur. J.* **2001**, *7*, No. 1

positions, and two of them belong to $N_3^-$ bridging ligands, which are also in the *trans* position. The $NiN_6$ core is a slightly distorted octahedron. The four N atoms of the diamine ligands and the $Ni^{II}$ atom are in the same plane. All the N–Ni–N angles in *trans* positions are 180°, and the $Ni–N_{azide}$ distances are 2.152(3) Å for Ni1 and 2.153(3) Å for Ni2, respectively. There are two different $Ni–N_{amine}$ distances for each different $Ni^{II}$ ion, the longer of these always corresponds to the $Ni–N_{amine}$ coordinated to the *Ethyl* ligand. The $Ni–N_{amine}$ bond lengths range from 2.073(4) to 2.148(4) Å. The $Ni–N_3–Ni$ torsion angle is 140.1°. The Ni–azido angles are $Ni–N_1–N_2 = 134.8$ and $Ni–N_3–N_2 = 123.4$.

*cis*-$[Ni(N\text{-}Eten)(\mu_{1,1}\text{-}N_3)_2]_n$ (***3***): The structure consists of neutral chains of nickel atoms linked by double EO azido bridges along the [0 0 1] axis (Figure 5). Two different [Ni(*N*-Eten)-

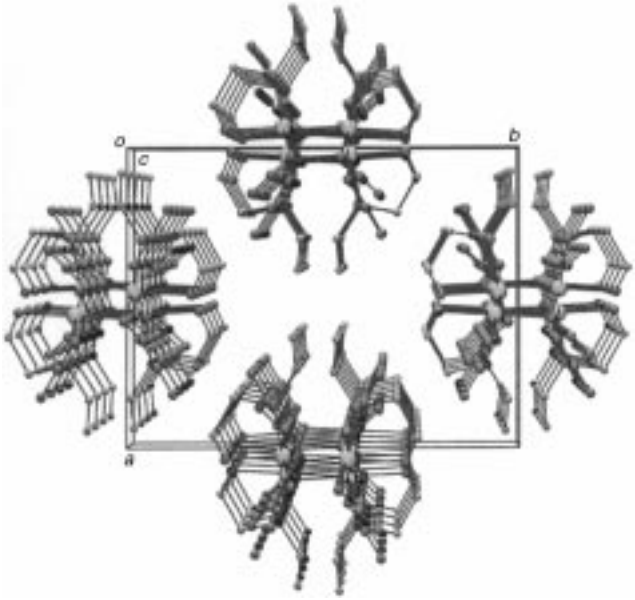


Figure 5. View of the unit cell of *cis*-$[Ni(N\text{-}Eten)(\mu_{1,1}\text{-}N_3)_2]_n$ (**3**). The hydrogen atoms are omitted for clarity.

$(\mu_{1,1}\text{-}N_3)_2]$ units may be found along the chain. In one of them, the $Ni^{II}$ atoms are related by an inversion center, and in the other the two metal ions are related by a twofold axis. An ORTEP plot of the basic unit of *cis*-$[Ni(N\text{-}Eten)(\mu_{1,1}\text{-}N_3)_2]_n$ is shown in Figure 6. Each $Ni^{II}$ ion is octahedrally coordinated to four different $N_3^-$ ligands and one *N*-Eten in the *cis* position. The $NiN_6$ octahedron is markedly distorted. The Ni1–N6–Ni1#2–N6#2 centro symmetric ring is planar and has a bond angle $Ni–N_{azido}–Ni = 103.3°$ and $Ni–N_{azido}$ distances of 2.127(2) and 2.105(19) Å. In this ring, the Ni–Ni distance is 3.3195(5) Å. The two azido ligands are parallel to each other and form an angle of 7° with the $Ni–N_{azido}–Ni–N_{azido}$ plane. The Ni1–N3–Ni1#1–N3#1 ring is not planar; the $Ni–N_{azido}–Ni$ angle is 100.6°, the $Ni–N_{azido}$ distances are 2.1382 and 2.172(2) Å, and the Ni–Ni distance is 3.3163(3) Å. The two azido ligands form, with the mean ring plane, an angle of 30.5°. The two different units are at an angle of 83.83° to each other as a consequence of their *cis* position; for this reason,

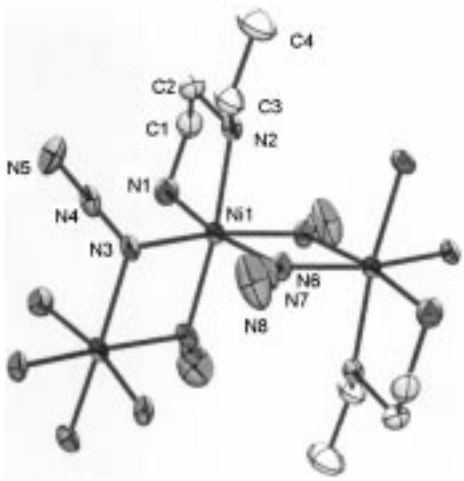


Figure 6. ORTEP view of *cis*-$[Ni(N\text{-}Eten)(\mu_{1,1}\text{-}N_3)_2]_n$ (**3**) with atomic numbering scheme and 50% thermal ellipsoids.

the chain is not completely parallel to the [0 0 1] crystallographic axis and has a zigzag skeleton. The shortest interchain $Ni\cdots Ni$ separation is 7.857 Å, and there are weak hydrogen bonds between the hydrogen of the amine of one chain and the uncoordinated nitrogen of the azide of the neighboring one {N1–H1N$\cdots$N5 [$3/2-x$, $3/2-y$, $1/2-z$] (H1N–N5 distance is 2.60(3) Å) and N2–H2N$\cdots$N8 [$5/2-x$, $y$, $-z$] (H2N–N8 distance is 2.52(2) Å)}. The main bond lengths and angles are gathered in Table 3.

Table 3. Selected bond lengths [Å] and angles [°] for [Ni(*N*-Eten)-$(\mu_{1,1}\text{-}N_3)_2]_n$ (**3**).

| | | | |
|---|---|---|---|
| Ni1–N1 | 2.115(2) | N4–N5 | 1.152(3) |
| Ni1–N2 | 2.104(2) | Ni1–N6 | 2.127(2) |
| Ni1–N3 | 2.138(2) | Ni1–N6#2 | 2.105(19) |
| Ni1–N3#1 | 2.172(2) | N6–N7 | 1.199(3) |
| N3–N4 | 1.201(3) | N7–N8 | 1.146(3) |
| N3–Ni1–N3#1 | 79.31(9) | N6–Ni1–N6#2 | 76.69(9) |
| Ni1–N3–Ni1#1 | 100.3(9) | Ni1–N6–Ni1#2 | 103.31(9) |
| N3–Ni1–N1 | 95.93(10) | N6–Ni1–N1 | 94.29(10) |
| N3–Ni1–N2 | 97.62(9) | N6–Ni1–N2 | 87.93(9) |
| N3#1–Ni1–N1 | 91.21(10) | N6#1–Ni1–N1 | 169.53(9) |
| N3#1–Ni1–N2 | 172.57(9) | N6#1–Ni1–N2 | 91.91(8) |
| N3–N4–N5 | 179.0(3) | N6–N7–N8 | 179.5(3) |
| Ni1–N3–N4 | 122.38(18) | Ni1–N6–N7 | 132.19(17) |
| Ni1#1–N3–N4 | 121.11(18) | N1#2–N6–N7 | 123.79(17) |
| N3–Ni1–N6 | 168.93(8) | N6–Ni1–N3#1 | 96.25(8) |
| N3–Ni1–N6#2 | 93.50(9) | N6#2–Ni1–N3#1 | 95.02(9) |
| N1–Ni1–N2 | 82.34(10) | | |

## Magnetic studies

*trans*-$[Ni(N\text{-}Eten)_2(\mu_{1,3}\text{-}N_3)]_n(ClO_4)_n$ (***1***): The magnetic data in the range 300–4 K are plotted in Figure 7. The $\chi_M T$ plot shows a regular decay from 0.9944 $cm^3 K mol^{-1}$ at room temperature and tends to zero when the temperature decreases. The molar susceptibility value ($3.429 \times 10^{-3}$ $cm^3 mol^{-1}$) increases when the temperature decreases; it reaches a maximum of $4.742 \times 10^{-3}$ at 105.5 K, and below this temperature the curve decreases continuously to 4 K. The continuous decrease in the $\chi_M T$ value and the position of the maximum observed in

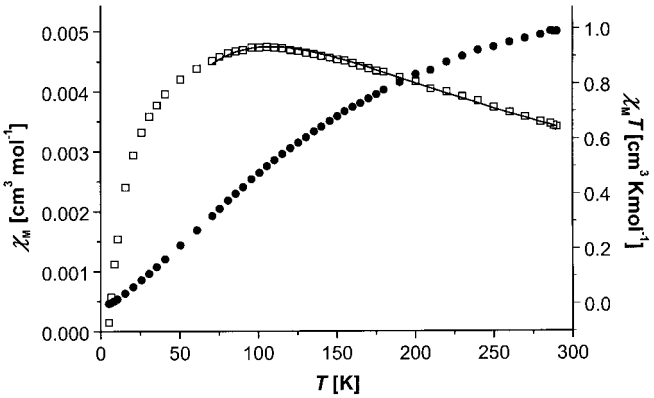


Figure 7. Plots of observed $\chi_M$ (□) and $\chi_M T$ (●) versus $T$ for *trans*-[Ni(*N*-Eten)$_2$($\mu_{1,3}$-$N_3$)]$_n$($ClO_4$)$_n$ (**1**). Solid line represents the best theoretical fit (see text).

the thermal variation of the $\chi_M$ clearly indicate the existence of strong antiferromagnetic intrachain interactions. If the existence of different azido bridges along the chain is taken into account, the experimental data can be fitted by using the Borras[14] expression for alternating antiferromagnetic chains; the value of the coupling parameters were optimized up to the values $J_1 = -68.4$ cm$^{-1}$, $J_2 = -37.6$ cm$^{-1}$ ($\alpha = J_2/J_1 = 0.55$), and $g = 2.38$. According to the structural data and the previous magneto structural correlation,[6] two very different values of $J$ are expected for the two different bridges. For both of these, the torsion angle is 180° (the optimum situation for the antiferromagnetic coupling), but the Ni–N–N angles are quite different. This situation permits the greater values of $J$ ($-68.4$ cm$^{-1}$) to be assigned to the bridge with a small angle (134.8°) and the lower values ($-37.8$ cm$^{-1}$) to the greater angle (147.7°). This correlation compares well with those reported in the literature.[5a]

*trans*-[*Ni*(*N-Eten*)$_2$($\mu_{1,3}$-$N_3$)]$_n$($PF_6$)$_n$ (***2***): The plot of the magnetic data in the 300–4 K range is shown in Figure 8. The general behavior corresponds to an antiferromagnetically coupled system, with a room-temperature $\chi_M T$ value of 1.14 cm$^3$ K mol$^{-1}$, which decreases continuously and tends to zero when the temperature decreases. $\chi_M$ shows a maximum at 18 K and then increases. The increase in the susceptibility

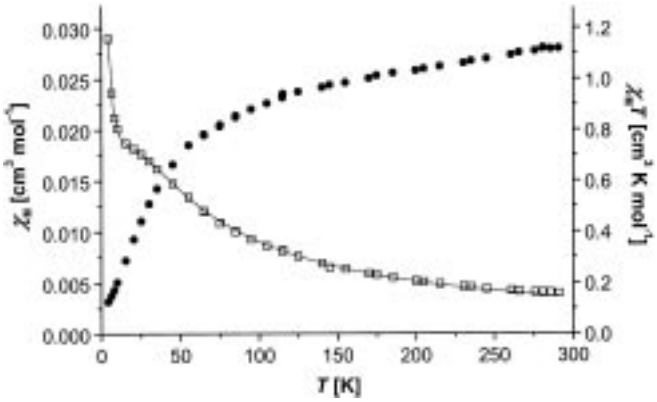


Figure 8. Molar magnetic susceptibility (□) and the $\chi_M T$ (●) product versus $T$ for *trans*-[Ni(*N*-Eten)$_2$($\mu_{1,3}$-$N_3$)]$_n$($PF_6$)$_n$ (**2**). Solid line shows the best fit obtained (see text).

when the compound cools down to very low temperature is most likely to be due to a small quantity of monomeric Ni$^{II}$ ions in the polycrystalline powder sample. According to the structural data, the existence of two kinds of Ni$^{II}$ ions and only one kind of azido bridge provides only one intramolecular coupling constant, $J$, and two different and alternating $g$ values. Taking into account the very small differences between the two Ni$^{II}$ environments, we interpreted the experimental data with an average $g$ value. The final expression of the susceptibility is shown in Equation (1).

$$\chi_M = \chi_{chain}(1-\rho) + \frac{2N\beta^2 g^2}{3kT}\rho \quad (1)$$

In Equation (1), we take into account the proportion, $\rho$, of a monomeric impurity, of which the susceptibility is assumed to follow Curie's law. $\chi_{chain}$ is the susceptibility of an infinite isotropic Heisenberg antiferromagnetic chain of $S = 1$ spin given by Weng.[16] Least-squares fitting of the experimental data led to the following values: $J = -13.6$ cm$^{-1}$, $g = 2.16$, and $\rho = 0.07$. In this case, the results are also comparable with those obtained for related compounds.[5] The position of the maximum indicates moderate antiferromagnetic coupling between Ni$^{II}$ ions through the $N_3^-$ bridge in agreement with the $J$ values. If we compare the values of the coupling constants obtained for **1** and **2**, we observe that the Ni–N–N angle is smaller for compound **2**, and this favors the magnetic coupling. However, the Ni–N3–Ni torsion angle for **1** is 180°, which is the optimum value for the magnetic coupling, and also the Ni–$N_{azide}$ distances are small, which is significant from the magnetic point of view. The experimental data are in agreement with the theoretical previsions.[6]

*cis*-[*Ni*(*N-Eten*)($\mu_{1,1}$-$N_3$)$_2$]$_n$ (***3***): The cryomagnetic behavior is shown in Figure 9. At room temperature, $\chi_M T$ is equal to 1.64 cm$^3$ K mol$^{-1}$ for all values of the applied field; a value slightly above that would be expected for isolated Ni$^{II}$ ions

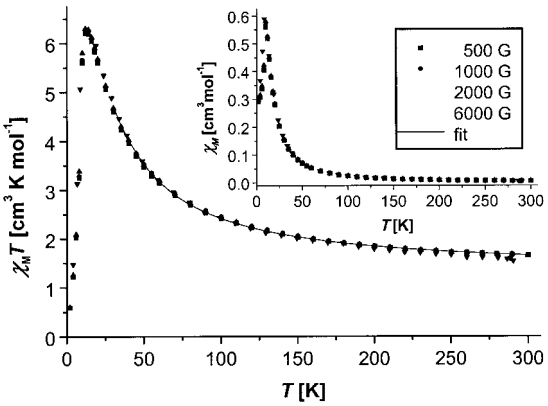


Figure 9. Plot of $\chi_M T$ versus temperature at four values of the applied field for *cis*-[Ni(*N*-Eten)($\mu_{1,1}$-$N_3$)$_2$]$_n$ (**3**). Solid line shows the best fit obtained (see text). Inset plot of $\chi_M$ versus temperature.

with local spin $S = 1$. $\chi_M T$ increases more and more rapidly as $T$ is lowered, then exhibits a very sharp maximum around 10 K with $\chi_M T = 6.3$ cm$^3$ K mol$^{-1}$ (the value of $\chi_M T$ and the temperature for the maximum remains unchanged for all



0947-6539/01/0701-0284 $ 17.50+.50/0 *Chem. Eur. J.* **2001**, *7*, No. 1

values of the applied field), and decreases as $T$ is lowered further. A maximum of $\chi_M$ is observed at $T_N = 10$ K. This behavior is characteristic of $Ni^{II}$ intrachain ferromagnetic interaction, with a long-range antiferromagnetic ordering of the ferromagnetic chains that occur at $T_N$. As a result of this antiferromagnetic interaction, the compound can be considered as a metamagnet.[17]

Further support for this comes from magnetization versus applied field plots at three temperatures (2, 5, and 10 K) from 0 to 50000 G (Figure 10). The curves at 2 and 5 K have the

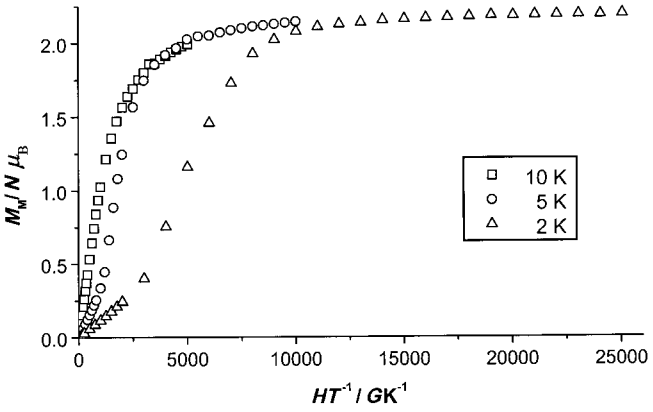


Figure 10. Magnetization versus applied field at three temperatures for *cis*-[Ni(*N*-Eten)($\mu_{1,1}$-$N_3$)$_2$]$_n$ (**3**).

sigmoidal shape (more markedly at lower temperature) expected for a metamagnet. Initially the magnetization increases slightly with increasing field because of antiferromagnetic interchain interactions. Subsequently it increases abruptly for a phase transition to a ferromagnetic state, and finally it reaches a saturation magnetization plateau around 2.1 $N\beta$, which corresponds to the value expected for a $Ni^{II}$ compound with all the local spins oriented along the field direction. The plot at 2 K exhibits a change of sign $\partial^2 M/\partial H^2$ at $Hc = 10$ KG; this value for the field is sufficient to overcome the weak antiferromagnetic interchain interaction and to lead to a ferromagnetic-like state.[18] The curve at 10 K ($T_N$) shows typical behavior for a ferromagnet.

To fit the magnetic data in the paramagnetic region, we developed a new mathematical expression.

**Magnetic model**: The Hamiltonian for the Heisenberg alternating ferro-ferromagnetic chain can be written as in Equation (2).

$$H = -\sum_{i=1}^{N-1} (J_1 S_{2i} S_{2i+1} + J_2 S_{2i} S_{2i-1}) \qquad (2)$$

In Equation (2), $N$ is the number of spin pairs. $J_1$ and $J_2$ are the nearest neighbor ferromagnetic exchange interactions; a positive $J$ means ferromagnetic coupling.

By applying the usual computational technique, based on the calculation of the properties of finite rings of increasing size ($N = 2$, 3, 4, and 5) and then extrapolating them to infinite, we have determined the product of the reduced susceptibility and reduced temperature ($\chi_r T_r$) (see below) of alternating ferro-ferromagnetic chains for different values of $\alpha$ ($\alpha = J_2/J_1$, $\alpha$ is between 0 and 1). In these calculations, we used the computer program *CLUMAG*, which uses the irreducible tensor operator formalism (ITO).[19] For example when $\alpha = 0.8$, we can see from Figure 11 the $\chi_r T_r$ curves of the chains when $N$ is 2, 3, 4, and 5 (solid line) and the infinite curve calculated by extrapolation (dashed line).

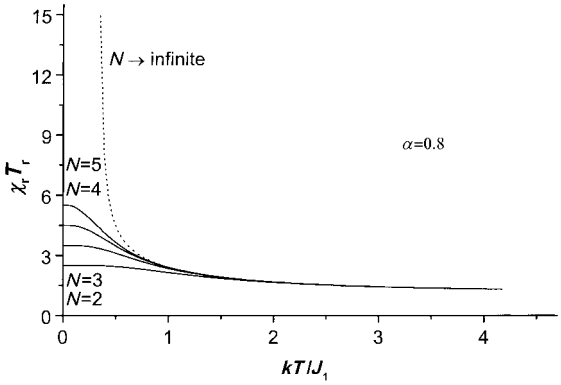


Figure 11. Theoretical curves of $\chi_r T_r$ versus $KT/J_1$.

The product $\chi_r T_r$, which depends on $T_r$, can be easily generated by applying the same strategy reported in the literature.[13] This involves the fitting of all the theoretical $\chi_r T_r$ curves ($N$ = infinite) with $\alpha = 0$, 0.1, 0.2, 0.4, 0.6, 0.8, and 1 to give the following rational expression in Equation (3).

$$\chi_r T_r = (A + BT_r + CT_r^2 + T_r^3)/(DT_r + ET_r^2 + T_r^3) \qquad (3)$$

In Equation (3), $\chi_r = (3/2)\chi_M J_1/Ng^2\beta^2$ and the reduced temperature $T_r$ is given by $kT/J_1$.

The $A-E$ values are the fitting coefficients, which depend on $\alpha$. Such dependence can be described by the use of the polynomial expression of second and third degree in $\alpha$ [Eqs. (4a) and (4b)].

$$Y_1 = x_{01}\alpha^2 + x_{11}\alpha + x_{21}, \text{ when } \alpha \text{ is between 0 and 0.4} \qquad (4a)$$

$$Y_2 = x_{02}\alpha^3 + x_{12}\alpha^2 + x_{22}\alpha + x_{32}, \text{ when } \alpha \text{ is between 0.4 and 1.0} \qquad (4b)$$

In these expressions, $Y_i$ can be $A-E$, and $x_{ii}$ is $a_{ii}-e_{ii}$. The two sets of coefficients proposed according to the values of $\alpha$ are reported in Table 4.

Table 4. Coefficients for the polynomials valid in the ranges $0 \le \alpha \le 0.4$ and $0.4 \le \alpha \le 1$.

| | $A$ | $B$ | $C$ | $D$ | $E$ |
|---|---|---|---|---|---|
| $0 \le \alpha \le 0.4$ | $a_{01} = -2.9718$ | $b_{01} = -4.8205$ | $c_{01} = 0.413168$ | $d_{01} = -1.02505$ | $e_{01} = -0.0161168$ |
| | $a_{11} = 1.72567$ | $b_{11} = -1.2537$ | $c_{11} = -2.54782$ | $d_{11} = -0.437735$ | $e_{11} = -3.14937$ |
| | $a_{21} = -0.037885$ | $b_{21} = 0.704729$ | $c_{21} = 1.20196$ | $d_{21} = 0.511936$ | $e_{21} = 0.529942$ |
| $0.4 \le \alpha \le 1$ | $a_{02} = -0.920563$ | $b_{02} = -0.42654$ | $c_{02} = 0.891021$ | $d_{02} = -1.12551$ | $e_{02} = 0.748354$ |
| | $a_{12} = 2.14971$ | $b_{12} = 1.33776$ | $c_{12} = -1.62232$ | $d_{12} = 2.48341$ | $e_{12} = -1.2567$ |
| | $a_{22} = -1.62319$ | $b_{22} = -1.57569$ | $c_{22} = 1.9104$ | $d_{22} = -1.84808$ | $e_{22} = 0.771037$ |
| | $a_{32} = 0.541133$ | $b_{32} = -0.124497$ | $c_{32} = -0.312675$ | $d_{32} = 0.586753$ | $e_{32} = -0.88762$ |

The product $\chi_r T_r$ can be converted to the product $\chi_M T$ in the habitual form to give Equation (5).

$$\chi_M T = (2/3)(Ng^2\beta^2/K)(AX^3 + BX^2 + CX + 1)/(DX^2 + EX + 1) \quad (5)$$

In this expression, $X = J_1/kT = 1/T_r$. The expression with the two sets of $A-E$ coefficients is valid for $T_r = KT/J_1 \geq 0.38$.

**Coupling constants calculations**: The experimental data were fit to the above equation in the range 300–30 K. With allowance for all the parameters to vary, the best least-square fit shown in Figure 9 gives $J_1 = 57.3\ cm^{-1}$, $J_2 = 29.0\ cm^{-1}$, $\alpha = 0.507$, $g = 2.26$, and $R = 1.2 \times 10^{-4}$. Despite the mathematical quality of the fit, the values of the coupling constants should be chemically reasonable in comparison with those for dinuclear compounds with a double EO bridge. All these complexes are coupled ferromagnetically and have a Ni–$N_{azido}$–Ni angle close to 101–105°. The $J$ values lie between 25–50 $cm^{-1}$.[5a] This result is also consistent with the calculations performed by Ruiz et al,[20] which predict a narrow range of the Ni–$N_{azido}$–Ni bond angle (±8°) around 104°, and minor $J$ differences should be expected.

## Conclusion

The reaction of $Ni(ClO_4)_2 \cdot H_2O$ or $Ni(NO_3)_2 \cdot H_2O$ (with or without $NH_4PF_6$) with *N*-Eten (*N*-Ethylethylenediamine) and $NaN_3$ in aqueous solution and in several ratios allowed the synthesis and characterization of three new one-dimensional complexes: *trans*-$[Ni(N\text{-Eten})_2(\mu_{1,3}\text{-}N_3)]_n(ClO_4)_n$ (**1**) consists of a structurally and magnetically alternating one-dimensional antiferromagnetic system with end-to-end azido bridges; *trans*-$[Ni(N\text{-Eten})_2(\mu_{1,3}\text{-}N_3)]_n(PF_6)_n$ (**2**) consists of structurally alternating but magnetically uniform one-dimensional antiferromagnetic system with end-to-end azido bridges; *cis*-$[Ni(N\text{-Eten})(\mu_{1,1}\text{-}N_3)_2]_n$ (**3**) consists of a structurally and magnetically alternating one-dimensional ferromagnetic system with double azido bridged ligands in end-on coordination mode. For the last of these systems, a new general formula for the magnetic susceptibility of the ferro-ferromagnetic $S = 1$ Heisenberg chain has been developed.

## Experimental Section

**Infrared spectra and magnetic measurements**: Infrared spectra (400–4000 $cm^{-1}$) were recorded from KBr pellets on a Nicolet 520 FTIR spectrophotometer. Magnetic measurements for **1** and **2** were carried out on polycrystalline samples with a pendulum type magnetometer (MANICS DSM8) equipped with a helium continuous-flow cryostat that worked in the temperature range 4–300 K and a Brucker BE15 electromagnet. The magnetic field was approximately 15000 G. For compound **3**, a Quantum Desing MPMS SQUID susceptometer that worked in the temperature range 300–2 K under a different external magnetic field (500, 1000, 2000, 6000 G) was used. Magnetization versus applied field measurements were made in the range 0 to 50000 G at temperatures of 2, 5, and 10 K. All magnetic measurements were performed on macroscopic crystals ground to a fine powder. Diamagnetic corrections were estimated from Pascal tables.

**Synthesis**: *Caution*! The azido and perchlorate complexes can be potentially explosive. Only a small amount of material should be prepared, and this should be handled with care.

***trans*-$[Ni(N\text{-Eten})_2(\mu_{1,3}\text{-}N_3)]_n(ClO_4)_n$ (1)**: A solution of *N*-Eten (0.35 g, 4 mmol) in water (20 mL) was added dropwise to a stirred aqueous solution (20 mL) of $Ni(ClO_4)_2 \cdot 6H_2O$ (0.73 g, 2 mmol), followed by the slow addition of a solution of $NaN_3$ (0.13 g, 2 mmol) in water (10 mL). The clear dark blue solution was filtered to remove any impurities and left to stand undisturbed at room temperature. Single blue crystals of **1** were collected after two weeks; the yield was approximately 75%. Elemental analysis calcd (%) for $C_8H_{24}ClN_7NiO_4$ (376.50): C 25.6, H 6.5, N 26.1; found C 25.5, H 6.5, N 26.2.

***trans*-$[Ni(N\text{-Eten})_2(\mu_{1,3}\text{-}N_3)]_n(PF_6)_n$ (2)**: An aqueous solution (10 mL) of $NaN_3$ (0.13 g, 2 mmol) was added slowly to a solution of $Ni(NO_3) \cdot 6H_2O$ (0.58 g, 2 mmol) and *N*-Eten (0.35 g, 4 mmol) in ethanol/water (1:1, 30 mL). After filtration to remove any impurities, $NH_4PF_6$ (0.40 g, 2.5 mmol) dissolved in water (15 mL) was added with continuous stirring. The solution was left undisturbed, and well-formed blue crystals of **2** were obtained after several days; the yield was approximately 70%. Elemental analysis calcd (%) for $C_8H_{24}F_6N_7NiP$ (422.02): C 22.8, H 5.7, N 23.3; found C 22.7, H 5.9, N 23.2.

***cis*-$[Ni(N\text{-Eten})(\mu_{1,1}\text{-}N_3)_2]_n$ (3)**: The new complex was synthesized by adding dropwise a solution of *N*-Eten (0.18 g, 2 mmol) in water (10 mL) to a stirred aqueous solution (20 mL) of $Ni(NO_3) \cdot 6H_2O$ (0.58 g, 2 mmol), followed by the slow addition of a solution of $NaN_3$ (0.26 g, 4 mmol) in water (10 mL). Then a dilute hydrochloric acid was added until a neutral pH was obtained. After a few minutes, a small quantity of greenish-white solid precipitated. This was filtered off and discarded. Slow evaporation of the clear dark green solution for three weeks at room temperature provided X-ray quality pale-green monocrystals; the yield was approximately 70%. Elemental analysis calcd (%) for $C_4H_{12}N_8Ni$ (230.95): C 20.9, H 5.3, N 48.7; found C 20.8, H 5.1, N 48.1.

**IR spectra**: In addition to the bands of the *N*-Eten, very strong bands corresponding to the characteristic $\nu_{as}$ of the azido ligand appeared at 2000–2150 $cm^{-1}$. This band appeared at about 2060 and 2100 $cm^{-1}$ for the EO and EE bridging modes, respectively.[21] For compounds **1** and **2**, it appeared at 2090 and 2080 $cm^{-1}$, respectively, while for **3** it split at 2065 and 2032 $cm^{-1}$. The $\nu_s$ mode was shown at 1300 $cm^{-1}$ only in the compound with EO bridging mode or in the compound where the EE mode was asymmetric. Only in compound **3** was the triplet band centered at 1300 $cm^{-1}$ attributable to the $\nu_s$ EO-azido group shown. The bands attributable to the perchlorate and hexafluorophosphate appeared at normal frequencies.

**Crystal structure determination**: Crystals of **1** (0.1 × 0.1 × 0.2 mm), of **2** (0.1 × 0.1 × 0.2 mm), and of **3** (0.45 × 0.25 × 0.10 mm) were selected and mounted on an MAR345 diffractometer with an image plate detector for **1**, on a Enraf-Nonius CAD4 four circle diffractometer for **2**, and on a Stoe Image Plate Diffraction System for **3**. The crystallographic data, conditions retained for the intensity data collection, and some features of the structure refinements are listed in Table 5. Unit cell parameters were determined

Table 5. Crystal data and structure refinement for *trans*-$[Ni(N\text{-Eten})_2(\mu_{1,3}\text{-}N_3)]_n(ClO_4)_n$ (**1**), *trans*-$[Ni(N\text{-Eten})_2(\mu_{1,3}\text{-}N_3)]_n(PF_6)_n$ (**2**), and *cis*-$[Ni(N\text{-Eten})(\mu_{1,1}\text{-}N_3)_2]_n$ (**3**).

| | **1** | **2** | **3** |
|---|---|---|---|
| formula | $C_8H_{24}ClN_7NiO_4$ | $C_8H_{24}F_6N_7NiP$ | $C_4H_{12}N_8Ni$ |
| $M_w$ | 376.50 | 422.02 | 230.95 |
| space group | $P2_1/c$ | $P\bar{1}$ | $I2/a$ |
| $a$ [Å] | 7.74000(10) | 8.301(7) | 10.5963(8) |
| $b$ [Å] | 17.54700(10) | 9.386(8) | 15.6922(10) |
| $c$ [Å] | 10.37100(10) | 11.8160(12) | 11.3429(10) |
| $\alpha$ [°] | 90 | 80.29 | 90 |
| $\beta$ [°] | 106.1030(1) | 83.72 | 96.094(10) |
| $\gamma$ [°] | 90 | 70.29 | 90 |
| $V$ [Å$^3$] | 1353.26(2) | 852.9(10) | 1875.4(2) |
| $Z$ | 4 | 2 | 8 |
| $T$ [°C] | 20(2) | 20(2) | 20(2) |
| $\rho_{calcd}$ [g cm$^{-3}$] | 1.848 | 1.643 | 1.636 |
| $\mu(Mo_{K\alpha})$ [mm$^{-1}$] | 1.662 | 1.297 | 1.954 |
| $R$ | 0.054 | 0.046 | 0.025 |
| $WR$ | 0.174 | 0.111 | 0.048 |



0947-6539/01/0701-0286 $ 17.50+.50/0 *Chem. Eur. J.* **2001**, *7*, No. 1

from automatic centering of 5368 reflections ($3 < \theta < 30^\circ$) for **1**, 25 reflections ($12 < \theta < 21$) for **2**, and 5000 reflections ($2.22 < \theta < 25.86^\circ$) for **3** and refined by least-squares methods. Intensities were collected with graphite monochromatized $Mo_{K\alpha}$ radiation using the $\varphi$ scan technique for **1** and **3**, and $\omega/2\theta$ for **2**. A total of 11013 reflections (3827 independent reflections $R_{int} = 0.048$) were collected for **1** in the range $2.35 < \theta < 39.70$, 2949 reflections (2949 independent reflections) for **2** in the range $2.33 < \theta < 24.96$, and 7243 reflections (1738 independent reflections $R_{int} = 0.054$) for **3** in the range $2.22 < \theta < 25.86^\circ$. 2256 reflections for **1**, 2209 for **2**, and 1214 for **3** were assumed as observed, if the condition $I > 2\sigma(I)$ was applied. Lorentz polarization was carried out. The crystal structures were solved by Patterson synthesis with the SHELXS-97 computer program[22] and refined by full matrix least-squares methods using the SHELXL-97 computer program.[23] The function minimized was $\Sigma w[|F_0|^2 - |F_c|^2]$ where $w = 1/[\sigma^2(F_0^2) + (0.1221P)^2]$ for **1**, $w = 1/[\sigma^2(F_0^2) + (0.0773P)^2]$ for **2**, and $w = 1/[\sigma^2(F_0^2) + (0.221\mathrm{P})^2]$ for **3** were $P = |F_0|^2 + 2|F_c|^2)/3$. Fourteen hydrogen atoms for **2** and twelve for **3** were located from a difference synthesis and refined with an isotropic temperature factor. The remaining H atoms for **1** and **2** were computed and refined isotropically using a riding model. The F atoms of compound **2** were disordered. The final $R$ factor was 0.054 ($WR2 = 0.174$) for **1**, 0.046 ($WR2 = 0.111$) for **2**, and 0.025 ($WR2 = 0.048$) for **3** using all observed reflections. Number of refined parameters were 212 (**1**), 323 (**2**), and 166 (**3**); maximum shift/esd = 0.00 for **1**, 0.003 for **2**, and 0.001 for **3**; maximum and minimum peaks in the final difference synthesis were 0.474 and $-0.441$ (**1**), 0.955 and $-0.908$ (**2**), and 0.242 and $-0.261$ (**3**) e $Å^{-3}$, respectively. Crystallographic data (excluding structure factors) for the structures reported in this paper have been deposited with the Cambridge Crystallographic Data Centre as supplementary publication nos. CCDC-143993 for **1**, CCDC-143994 for **2**, and CCDC-143995 for **3**. Copies of the data can be obtained free of charge on application to CCDC, 12 Union Road, Cambridge CB21EZ, UK (Fax: (+44) 1223-336-033; e-mail: deposit@ccdc.cam.ac.uk.).

## Acknowledgements

This work was supported by the Spanish Dirección General de Investigación Científica y Técnica (project PB96-0163). I.R. thanks the Ministerio de Educacion y Cultura for a doctoral FPI fellowship.

[1] W.-E. Hatfield, W.-E. Estes, W.-E. Marsh, M.-W. Pickens, L.-W. ter Haar, R.-R. Weller in *Extended Linear Chain Compounds*, *Vol. 3* (Eds.: J. S. Miller), Plenum, New York, **1983**, p. 43.

[2] J.-C. Bonner in *Magneto-Structural Correlations in Exchange Coupled Systems*, *NATO ASI Series* (Eds.: R.-D. Willet, D. Gatteschi, O. Kahn), Reidel, Dordrecht, **1984**.

[3] *Physics in One Dimension* (Eds.: J. Bernasconi, T. Schneider), Springer, Berlin, **1981**.

[4] *Organic and Inorganic Low-Dimensional Crystalline Materials*, *Vol B168* (Eds.: P. Delhaes, M. Drillon), Plenum, New York, **1987**.

[5] a) J. Ribas, A. Escuer, M. Monfort, R. Vicente, R. Cortés, L. Lezama, T. Rojo, *Coord. Chem. Rev.* **1999**, 193; J. Ribas, A. Escuer, M. Monfort, R. Vicente, R. Cortés, L. Lezama, T. Rojo, *Coord. Chem. Rev.* **1999**, 1027; b) L.-F. Tang, L. Zhang, L.-C. Li, P. Cheng, Z.-H. Wang, J.-T. Wang, *Inorg. Chem.* **1999**, *38*, 6326; c) H.-Y. Shen, W.-M. Bu, E.-Q. Gao, D.-Z. Liao, Z.-H. Jiang, S.-P. Yan, G.-L. Wang, *Inorg. Chem.* **2000**, *39*, 396.

[6] A. Escuer, R. Vicente, J. Ribas, M.-S. El Fallah, X. Solans, M. Font-Bardia, *Inorg. Chem.* **1994**, *33*, 1842.

[7] C.-S. Hong, Y. Do, *Angew. Chem.* **1999**, *111*, 153; *Angew. Chem. Int. Ed.* **1999**, *38*, 193.

[8] M.-A.-M. Abu-Youssef, A. Escuer, D. Gatteschi, M.-A.-S. Goher, F. A. Mautner, R. Vicente, *Inorg. Chem.* **1999**, *38*, 5716.

[9] M.-E. Fisher, *Am. J. Phys.* **1964**, *32*, 343.

[10] J.-L. Manson, A.-M. Arif, J.-S. Miller, *Chem. Commun.* **1999**, 1479.

[11] J. Ribas, M. Monfort, C. Diaz, C. Bastos, X. Solans, *Inorg. Chem.* **1994**, *33*, 484.

[12] T. de Neef, PhD thesis, Eindhoven (Netherlands), **1975**.

[13] J.-W. Hall, W.-E. Marsh, R.-R. Welles, W.-E. Hatfield, *Inorg. Chem*, **1981**, *20*, 1033.

[14] J.-J. Borras-Almenar, E. Coronado, J. Curely, R. Georges, J.-C. Gianduzzo, *Inorg. Chem.* **1994**, *33*, 5171; J.-J. Borras-Almenar, E. Coronado, J. Curely, R. Georges, J.-C. Gianduzzo, *Inorg. Chem*, **1995**, *34*, 2699.

[15] A. Escuer, R. Vicente, M.-S. El Fallah, S.-B. Kumar, F.-A. Mautner, D. Gatteschi, *J. Chem. Soc. Dalton Trans.* **1998**, 3905

[16] C.-Y. Weng, PhD thesis, Carnegie Institute of Technology (US), **1968**.

[17] O. Kahn, E. Bakalbassis, C. Mathonière, M. Hagiwara, K. Katsumata, L. Ouahab, *Inorg. Chem.* **1997**, *36*, 1530.

[18] R.-D. Willet, R.-M. Gaura, C.-P. Landee in *Extended Linear Chain Compounds*, *Vol 3* (Eds.: J. S. Miller), Plenum, New York, **1983**, p. 143.

[19] D. Gatteschi, P. Luca, *Gazz. Chim. Ital.* **1993**, *123*, 231.

[20] E. Ruiz, J. Cano, S. Alvarez, P. Alemany, *J. Am. Chem. Soc.* **1998**, *120*, 11122.

[21] R. Cortés, M. Drillon, X. Solans, L. Lezama, T. Rojo, *Inorg. Chem.* **1997**, *36*, 677.

[22] G.-M. Sheldrick, *SHELXL-97*, *Program for the Solution for Crystal Structure*, Universität Göttingen, Germany, **1997**.

[23] G.-M. Sheldrick, *SHELXL-97*, *Program for the Refinement of Crystal Structure*, Universität Göttingen, Germany, **1997**.

Received: May 18, 2000 [F2499]